A zonal advection-diffusion-reaction model for self-disturbance correction in point-particle computations

By S. V. Apte†

A novel approach to correct for the self-disturbance created by a particle in two way–coupled point-particle computations is developed. The self-disturbance velocity field is obtained by solving the model advection-diffusion-reaction (ADR) equations for each particle, in a small zone of interest, using an overset grid–based approach. This zonal solution of the ADR equations is then used to construct the undisturbed fluid velocity needed in force closure models. The Zonal-ADR model is first verified for a range of single- and multiple-particle test cases including isotropic turbulence laden with Kolmogorov-scale particles to show good predictions compared to available data. The model is applicable over a range of Reynolds numbers, wall-bounded flows, and different interpolation kernels.

1. Introduction

The Euler-Lagrange particle-laden flow simulations typically employ the point-particle model, wherein the flow around the particle is not resolved and the particles are assumed to be subgrid point sources. The coupling force between the fluid and the particles is evaluated using empirical closure models for drag, lift, added mass, pressure, and history forces, among others (Maxey 1987). The reaction force from the particles is distributed to the neighboring grid control volumes and added to the fluid momentum equations. The force closure models for low volume loadings are typically based on the undisturbed fluid velocity seen by the particle, which is defined as the fluid velocity at the particle location in the absence of the self-disturbance created by the particle under consideration. This undisturbed fluid velocity is not readily available in a two way–coupled computation. Instead, the disturbed fluid flow is typically used. When the particles are much smaller than the Eulerian grid, the magnitude of the self-disturbance velocity field is small, and does not significantly affect the fluid velocity in neighboring control volumes. The Euler-Lagrange point-particle approach then provides reasonably accurate predictions of the particle dynamics and fluid-particle interactions. However, several applications involving sprays and droplet breakup (Apte *et al.* 2003) and wall-bounded channel flows (Gualtieri *et al.* 2015; Horwitz *et al.* 2022) result in particles that are on the order of the Eulerian grid in one or more directions. Under such situations, the point-particle approach can result in large errors when the self-disturbance field is neglected (Gualtieri *et al.* 2015; Horwitz & Mani 2018).

Obtaining the undisturbed fluid flow has received significant attention recently (Gualtieri *et al.* 2015; Ireland & Desjardins 2017; Horwitz & Mani 2018; Esmaily & Horwitz 2018; Balachandar *et al.* 2019; Evrard *et al.* 2020; Pakseresht *et al.* 2020; Pakseresht & Apte 2021; Horwitz *et al.* 2022). A majority of these methods use the analytical Stokes flow solution over a particle in an unbounded domain (Ireland & Desjardins 2017; Esmaily

† School of Mechanical, Industrial, and Manufacturing Engineering, Oregon State University

& Horwitz 2018; Horwitz & Mani 2018), Oseen-like discrete Green's functions (Horwitz *et al.* 2022), or the Stokeslet solution for wall-bounded flows (Pakseresht *et al.* 2020), and have been shown to be effective at low particle Reynolds numbers ($Re_p \leq 20$, approximately). Balachandar *et al.* (2019); Liu *et al.* (2019) and (Evrard *et al.* 2020) used a regularized Green's function with extensions to higher Reynolds numbers using Oseen's approximation and other correction factors.

Pakseresht & Apte (2021) derived the equations for disturbances created by a single particle and solved it directly using an approximation for the pressure disturbance to show good results for a range of Reynolds numbers. However, their approach did not include the neighboring particle disturbances. In this work, the approach first developed by Pakseresht & Apte (2021) is extended to multiple particle systems by using an overset grid for solution of the disturbance field around each particle. The undisturbed velocity seen by each particle includes the disturbances from all other particles and thus the formulation is able to capture the effect of neighboring particles.

The rest of the paper is arranged as follows. The mathematical formulation for the disturbance field is derived in Section 2. Section 3 briefly describes the zonal implementation of disturbance field solution for each particle. Section 4 documents verification studies for a range of standard test cases for single- and multiple-particle systems including particle-laden decaying isotropic turbulence corresponding to the particle-resolved direct numerical simulation (PR-DNS) of Mehrabadi *et al.* (2018), followed by a summary in Section 5.

2. Mathematical formulation

The mathematical formulation is based on the incompressible Navier-Stokes equations,

$$\frac{\partial u_j}{\partial x_j} = 0, \tag{2.1}$$

$$\rho_g \left(\frac{\partial u_i}{\partial t} + \frac{\partial u_i u_j}{\partial x_j} \right) = -\frac{\partial p}{\partial x_i} + \mu \frac{\partial^2 u_i}{\partial x_j^2} + \underbrace{\left(-\sum_{q=1}^{N_p} \mathcal{G}^\sigma(\mathbf{x}_{cv} - \mathbf{x}_q) F_{i,q}^t \right)}_{\dot{S}_i}, \tag{2.2}$$

where ρ_g is the density of the fluid, μ is the dynamic viscosity, p is the pressure, and u_i is the two-way coupled fluid velocity that includes the disturbances created by all N_p particles through the net interphase source term ($\dot{S}_i$) based on all forces ($F_{i,q}^t$), except the gravity, acting on the particle located at $\mathbf{x}_q$ and projected onto the Eulerian grid control volumes located at $\mathbf{x}_{cv}$, using the interpolation kernel $\mathcal{G}^\sigma$, with σ being the kernel width. The projection function satisfies the conservation condition, $\int_{\mathcal{V}} \mathcal{G}^\sigma d\mathcal{V} = 1$, where the integration is over the whole fluid volume ($\mathcal{V}$).

The undisturbed flow field seen by a particle p [denoted by superscript $(\cdot)^{u,p}$] can be obtained by excluding the reaction force from the p^{th} particle,

$$\frac{\partial {u_j}^{u,p}}{\partial x_j} = 0, \tag{2.3}$$

$$\rho_g \left(\frac{\partial {u_i}^{u,p}}{\partial t} + \frac{\partial {u_i}^{u,p} {u_j}^{u,p}}{\partial x_j} \right) = -\frac{\partial p^{u,p}}{\partial x_i} + \mu \frac{\partial^2 u_i^{u,p}}{\partial x_j^2} - \sum_{q=1, q\neq p}^{N_p} \mathcal{G}^\sigma(\mathbf{x}_{cv} - \mathbf{x}_q) F_{i,q}^t. \tag{2.4}$$

Subtracting Eqs. (2.1)-(2.2) from the corresponding Eqs. (2.3)-(2.4), the self-disturbance

field [denoted by superscript $(\cdot)^{d,p}$] created by the particle p is given as

$$\frac{\partial u_j^{d,p}}{\partial x_j} = 0, \tag{2.5}$$

$$\rho_g \left(\frac{\partial u_i^{d,p}}{\partial t} + \frac{\partial u_j u_i^{d,p}}{\partial x_j} + \frac{\partial u_j^{d,p} u_i^{u,p}}{\partial x_j} \right) = -\frac{\partial p^{d,p}}{\partial x_i} + \mu \frac{\partial^2 u_i^{d,p}}{\partial x_j^2} + \mathcal{G}^\sigma(\mathbf{x}_{cv} - \mathbf{x}_q) F_{i,p}^t, \tag{2.6}$$

where

$$u_i^{d,p} = u_i^{u,p} - u_i, \quad p^{d,p} = p^{u,p} - p. \tag{2.7}$$

Note that in the self-disturbance equation, only the interaction force from the particle p is needed. There is also nonlinear interaction between the disturbance field for particle p and the two way–coupled velocity (u_i) as well as the undisturbed velocity ($u_i^{u,p}$).

Solving the above set of equations, although possible, is expensive, as it requires solution of a Poisson system for the pressure disturbance for each particle. Pakseresht & Apte (2021) first suggested to approximate the pressure and viscous terms in the disturbance equation as a diffusion term with effective viscosity $K_\mu \mu$. The idea for such approximation stems from the fact that in the Stokes flow limit, the pressure contribution to the drag force on a spherical particle is exactly half of the viscous contribution and has the same form as the viscous force. Hence, to match the drag force in the Stokes limit, $K_\mu = 1.5$ was used. In general, K_μ will vary based on the Reynolds number. Recent PR-DNS studies by Ganguli & Lele (2019) showed that the ratio of pressure to viscous contribution to drag remains roughly the same up to a particle Reynolds number of 10. Hence, $K_\mu = 1.5$ is used for all cases considered in this work, and good predictions up to $Re_p = 100$, suggest that the assumption is reasonable even for larger Reynolds numbers.

The approximate disturbance equations for the particle p then become

$$\rho_g \left(\frac{\partial u_i^{d,p}}{\partial t} + \frac{\partial u_j u_i^{d,p}}{\partial x_j} + \frac{\partial u_j^{d,p} u_i^{u,p}}{\partial x_j} \right) = K_\mu \mu \frac{\partial^2 u_i^{d,p}}{\partial x_j^2} + \mathcal{G}^\sigma(\mathbf{x}_{cv} - \mathbf{x}_q) F_{i,p}^t. \tag{2.8}$$

The above nonlinear, unsteady advection-diffusion-reaction (ADR) equations are solved in addition to Eqs. (2.1-2.2), to obtain the undisturbed velocity from Eqs. (2.7).

The Lagrangian equations for the motion of the p^{th} particle are

$$\frac{dx_{i,p}}{dt} = u_{i,p}, \quad m_p \frac{du_{i,p}}{dt} = m_p \left(1 - \frac{\rho_g}{\rho_p}\right) g_i + F_{i,p}^t, \tag{2.9}$$

where $x_{i,p}$ and $u_{i,p}$ are the particle position and velocity, respectively; m_p is the mass of the particle, and $F_{i,p}^t$ represents forces acting on the particle including the drag, lift, added mass, pressure, and history, among others. For example, the standard drag force on the particle p can be modeled as,

$$F_{i,p}^{\text{drag}} = m_p \frac{u_{i,@x_p}^{u,p} - u_{i,p}}{\tau_r}, \quad \tau_r = \frac{1}{f} \frac{\rho_p D_p^2}{18\mu}, \quad f = 1 + 0.16 Re_p^{0.687}, \tag{2.10}$$

where $u_{i,@\mathbf{x}_p}^{u,p}$ represents the undisturbed fluid velocity seen by the particle p and interpolated to the particle location ($\mathbf{x}_p$), D_p is the particle diameter, τ_r is the particle relaxation time, and f is the Schiller and Naumann nonlinear correction for drag coefficient based on the particle Reynolds number, $Re_p = \rho_g D_p |u_{i,@\mathbf{x}_p}^{u,p} - u_{i,p}|/\mu$.

A grid resolution–based, compact, three-point Roma-delta function is used as kernel to interpolate the flow variables from the control volume centers to the particle locations,

and to project source terms from the particle location to the surrounding control volumes. The kernel is second-order, smoother than trilinear interpolation, and commonly used in immersed-boundary methods (Roma *et al.* 1999)

$$\mathcal{G}^{\Delta}(\mathbf{x}_{cv}-\mathbf{x}_p) = \begin{cases} \frac{1}{6}(5-3|r|-\sqrt{-3(1-|r|)^2+1}), & 0.5 \le |r| \le 1.5, r = |\mathbf{x}_{cv}-\mathbf{x}_p|/\Delta \\ \frac{1}{3}(1+\sqrt{-3r^2+1}), & |r| \le 0.5 \\ 0, & \text{otherwise.} \end{cases} \tag{2.11}$$

3. The Zonal-ADR method

The ADR equations for each particle p only need the net force acting on the particle $F^t_{i,p}$ and can be solved separately. In addition, the undisturbed fluid velocity is only needed at the particle location to compute the particle forces. These two aspects are exploited by solving the ADR equations in a small zone surrounding the particle.

A Cartesian, collocated grid–based, second-order, fractional time–stepping solver has been developed (Finn *et al.* 2016) and used in the present work. An overset-grid algorithm is devised for the zonal solution. In general, the solution of the ADR equation can be carried out on a grid not aligned with the flow-solver grid. However, this requires interpolation of the two way–coupled fluid velocity from the flow-solver grid to the overset grid, resulting in interpolation errors. In the present case, the overset grid and the flow-solver grids are exactly aligned, and only the control volumes where the ADR equations need to be solved for each particle are tagged (see Figure 1). As the particle moves, this tag for flow-solver control volumes is updated at each time step. A zone containing $\pm cni$, $\pm cnj$, $\pm cnk$ control volumes is used, where cni, cnj, and cnk correspond to the extent of the number of overset-grid points around the particle in x, y, and z directions, respectively. Typically, the values of cni, cnj, and cnk depend on the particle size as well as the local grid resolution. A typical value of ±6–8 grid points is found to be sufficient for all the test cases studied in the present work.

The second term in the ADR Eq. (2.8) represents advection of the disturbance by the two way–coupled velocity field (u_i). This velocity field is already known from the solution of the two way–coupled Navier-Stokes equations (2.2). The continuity-satisfying, face-based velocity field and the cell-center velocity (u_i) are needed for each tagged control volume. If the zone corresponding to a particle q crosses over processor boundaries, transfer of cell-center and face-based velocity for several ghost cells is needed from neighboring processors. The number of ghost cells in each direction is thus set equal to cni, cnj, and cnk, respectively. The third term in the ADR Eq. (2.8) represents advection of the undisturbed flow velocity ($u_i^{u,p}$) by the disturbance field. This nonlinear term is treated explicitly by using the undisturbed flow velocity from the previous iteration. Improved temporal accuracy for this term can be obtained using multiple inner iterations; however, it was found to be unnecessary for the cases studied. The viscous and the other advection term are approximated using the second-order Crank-Nicholson scheme and using the same spatial discretization algorithm as the baseline flow solver.

The disturbance field diminishes to zero far away from the particle. If there are walls present in the domain, the disturbance velocity field at the wall also goes to zero due to no-slip condition. Thus, obtaining the disturbance field for a particle near a wall is straighforward by simply imposing the no-slip condition. The disturbance field is generated by the particle reaction force and in the absence of any advection, it is simply diffused away from the particle. In the presence of advection, a convective outflow bound-

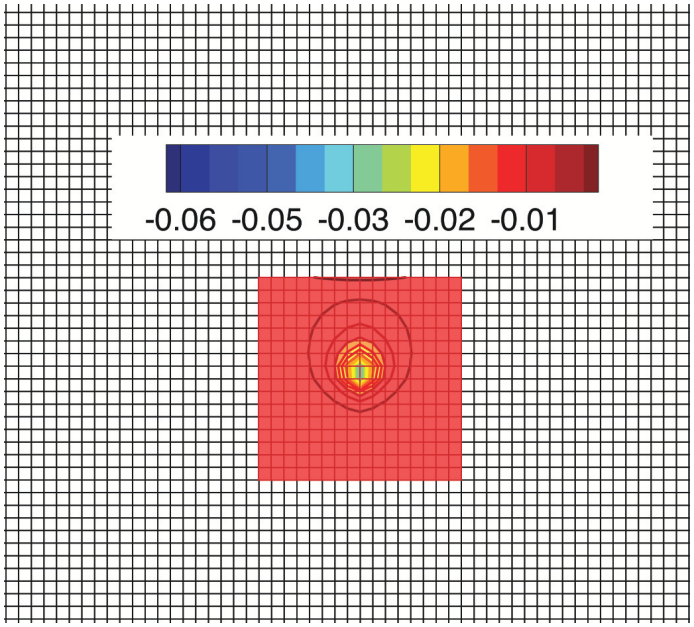

FIGURE 1. Zonal-ADR solution on ±8 overset grids around the particle center. The flow-solver and overset grids and the computed disturbance velocity in the vertical direction are shown for a particle settling under gravity.

ary condition is applied on boundaries of the overset grid that has outflux due to the two way–coupled velocity field, whereas no new disturbance is introduced at the influx boundaries. The complete algorithm for each time step can be summarized as follows:

(a) Solve the Lagrangian particle Eqs. (2.9) using the undisturbed fluid velocity. Advance the particle locations, and update the particles across processors.

(b) Project the net force on all particles ($F^t_{i,q}$, $q = 1, .., N_p$) onto the Eulerian grid.

(c) Solve the two way–coupled Navier-Stokes Eqs. (2.2) using the fractional time-stepping, collocated-grid algorithm to obtain the velocity, u_i, and pressure, p.

(d) Update the cell-center and face-based velocities across processors for the overset grid used by each particle.

(e) Sequentially solve the ADR Eq. 2.2) over the overset mesh for each particle and obtain the disturbance field ($u_i^{d,p}$). Compute the undisturbed fluid velocity using Eq. (2.7) over the overset grid and interpolate it to the particle location.

The Zonal-ADR approach requires storage of the two-way coupled velocity field on the overset grid for each particle. Using only a few grid cells around the particle, the solution of the ADR equations is reasonably fast and its overhead is insignificant, with proper particle-load balancing. The ADR equation for each particle is independent of other particles, and thus the method is suitable for graphics processing unit (GPU)-based acceleration.

TABLE 1. Percentage relative error in undisturbed fluid velocity at particle location for flow over a stationary particle using the uncorrected, the Zonal-ADR (with ±8 cells around particle), and the Esmaily & Horwitz (2018) (E&H) method implemented in the present collocated solver.

Re_p	Uncorrected	Zonal-ADR	E&H
0.1	57	1.2	1.05
0.5	53	0.5	0.83
1	34	0.87	4.5
10	14	1.7	6.8
100	9	0.9	-

4. Results

The Zonal-ADR model for self-disturbance correction is verified for a range of single- and multiple-particle test cases and the results are compared against other approaches.

4.1. *Flow over a stationary sphere*

Flow over a stationary particle is investigated for a range of particle Reynolds numbers ($0.1 \leq Re_p \leq 100$). Particle of size $D_p = 1/100$ is placed at the center of a cubic domain of unit length. A grid resolution of $\Delta = D_p$ is used in all directions. Percentage errors in the undisturbed fluid velocity at the particle location obtained with (i) no model, (ii) the Zonal-ADR model, and (iii) the E&H (Esmaily & Horwitz 2018) model implemented in the present collocated-grid solver are shown in Table 1. The Zonal-ADR approach uses the grid-based Roma interpolation kernel, whereas the E&H approach uses the trilinear interpolation for both the Euler-to-Lagrange (E2L) and Lagrange-to-Euler (L2E) interpolations. The present correction model significantly reduces the error in undisturbed fluid velocity compared to the uncorrected two way–coupled calculation for a wide range of Reynolds numbers. The E&H model produces good results for $Re_p \leq 10$; however, it produces errors comparable to the uncorrected model at higher Reynolds numbers, as it assumes Stokes flow and is applicable at low Re_p.

4.2. *Settling particle parallel to a wall*

Verification of settling speed of a particle falling freely under gravity in a quiescent fluid and parallel to a wall at $Re_p = 1$ is considered, following the work of Horwitz *et al.* (2022). A spherical particle settles parallel to a no-slip wall at different distances from the wall. Owing to the disturbance created by the particle near the wall, the particle experiences force normal to the wall. However, the particle is constrained to move parallel to the wall, and the settling speed of the particle is compared with the one way–coupled settling speed. Percentage errors in settling speed for particles settling at different normalized distances $[\ell/(0.5D_p)]$ are shown in Figure 2 for a uniform grid with $D_p/\Delta = 2$, and compared with predictions made by Esmaily & Horwitz (2018), Horwitz *et al.* (2022), and the uncorrected scheme. The present Zonal-ADR model is able to correct for the disturbance created by the particle next to a wall fairly accurately without requiring any special treatment to account for the wall-bounded disturbance.

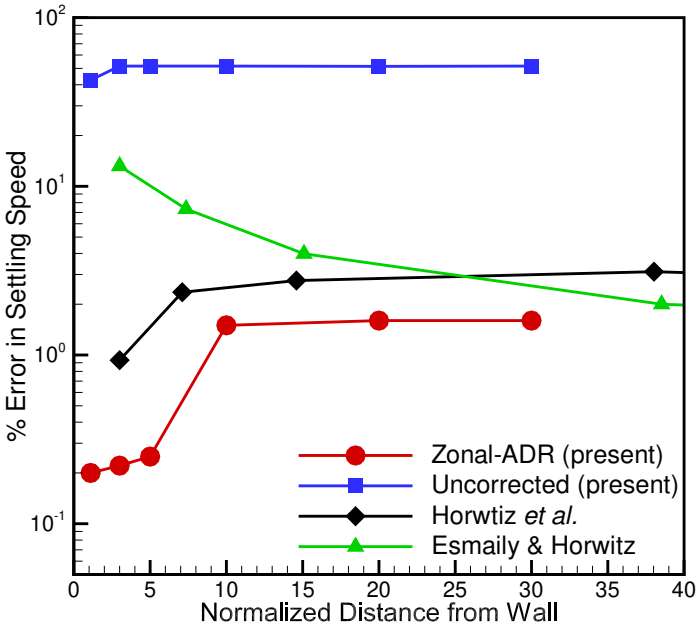

FIGURE 2. Percentage error in settling speed of a particle parallel to a no-slip wall at different normalized distances from the wall predicted by the present Zonal-ADR, uncorrected, Horwitz *et al.* (2022), and Esmaily & Horwitz (2018) models.

TABLE 2. Percentage error in settling speed of two touching particles ($\ell/D_p = 1$) settling side by side in a quiescent fluid at $Re_p = 0.1$ using uncorrected two way–coupled computation and the Zonal-ADR method with Roma interpolation kernel, and the Esmaily & Horwitz (2018) (E&H) model with trilinear interpolation implemented in the present collocated-grid solver.

D_p/Δ	Uncorrected	Zonal-ADR	E&H
0.5	19.3	3.2	4.3
1	53	2.1	1.5
1.5	75	0.9	1.2
3	91	5.2	5.1

4.3. *Settling of two particles*

The test case of two particles falling side by side under gravity in a quiescent fluid investigated by Esmaily & Horwitz (2018) is considered to test the capability of the Zonal-ADR model to capture the effect of disturbance fields created by neighboring particles. The degree to which the settling velocity changes depends on the distance (ℓ) between the two particles. Particles at infinite distance will have no effect on settling speed of one another, whereas as the separation distance is reduced, the settling speed

of the group increases, with the largest modification occurring when two particles are touching each other at $\ell = D_p$. Under free fall, two side by side particles will experience a drag force as well as a repulsive force normal to their settling velocity. However, to facilitate comparison with the analytical solution, the distance between the particles is kept constant, and the particles are constrained to move parallel to each other.

At a terminal settling Reynolds number of $Re_p = 0.1$ for a single particle, the group settling speed becomes $1.38U_s$, where U_s is the settling speed of a single particle in an unbounded domain (Esmaily & Horwitz 2018). For the present test case, the particle-to-fluid density ratio is 180, particle diameter is $D_p = 1/100$, viscosity $\mu = 0.001$, and gravitational acceleration g =-0.01 giving a Stokes number of 10 and Reynolds number based on the terminal speed of a single particle of 0.1. The predictions from the Zonal-ADR model are compared with no correction as well as the Esmaily & Horwitz (2018) model (E&H) and the percentage errors are shown in Table 2. The uncorrected approach overpredicts the settling speed. The Zonal-ADR approach is able to capture the group settling speed accurately for different particle sizes relative to the grid size and results are comparable to the E&H model implemented in the present solver.

4.4. *Decaying isotropic turbulence*

Decaying isotropic turbulence laden with Kolmogorov-scale particles is simulated corresponding to the particle-resolved data by Mehrabadi *et al.* (2018) at a Taylor microscale Reynolds number of $Re_\lambda \sim 27$. The computational domain is a triply periodic cubic box of side length 2π. The initial condition for each case is the divergence-free random field sampled from Pope's model energy spectrum (Pope 2000). The particle size (D_p) is selected to be same as the initial Kolmogorov length scale, $\eta_0 = 2\pi/96$. The grid resolution used is finer than the particle size ($D_p/\Delta = 2$) to assess the ability of the Zonal-ADR model to predict the undisturbed flow field for particle sizes larger than the grid. The particle density ratio is $\rho_p/\rho_f = 1800$, particle Stokes number $St_p = (1/18)(\rho_p/\rho_f)(D_p/\eta_0)^2 = 100$, while the volume and mass loading are $\phi = 0.001$ and $\phi_m = 1.8$, respectively, giving a total of $N_p = 1689$ particles in the domain. Particle dynamics are based only on drag force modeled using the standard Schiller-Naumann drag correlation. Initially, particles are injected at random positions within the domain, and the initial particle velocity is set equal to the fluid velocity interpolated to the particle center. Figure 3(a) shows the instantaneous snapshot of out-of-plane vorticity superimposed by particles in the plane. The particles are colored by the disturbance velocity at the particle location. Figure 3(b) shows the temporal evolution of particle kinetic energy normalized by the initial fluid phase kinetic energy obtained using the grid-based Roma interpolation kernel with and without any self-disturbance correction. Also shown is the prediction using the Esmaily & Horwitz (2018) model with trilinear interpolation kernel implemented in the present solver. Without any correction model, the fluid velocity at the particle location used in the drag model is incorrect, resulting in underprediction of the drag force and hence significantly lower damping of the particle kinetic energy. With correction, both models reproduce the PR-DNS data by Mehrabadi *et al.* (2018).

Figure 3(c) shows the temporal evolution of the net dissipation rate normalized by the initial dissipation rate $[\varepsilon^{(net)}/\varepsilon_0^{(f)}]$ for the various interpolation kernels with and without correction. The net dissipation rate is computed as the rate of change of the mixture kinetic energy of the system, $\varepsilon^{(net)} = -de_m/dt = -\left[(1-\phi)\rho_f dk^{(f)}/dt + \phi\rho_p dk^{(p)}/dt\right]$, where $k^{(f)}$ and $k^{(p)}$ represent the volume-averaged fluid and particle kinetic energy, respectively. Without correction for self-disturbance, the net dissipation rate is significantly

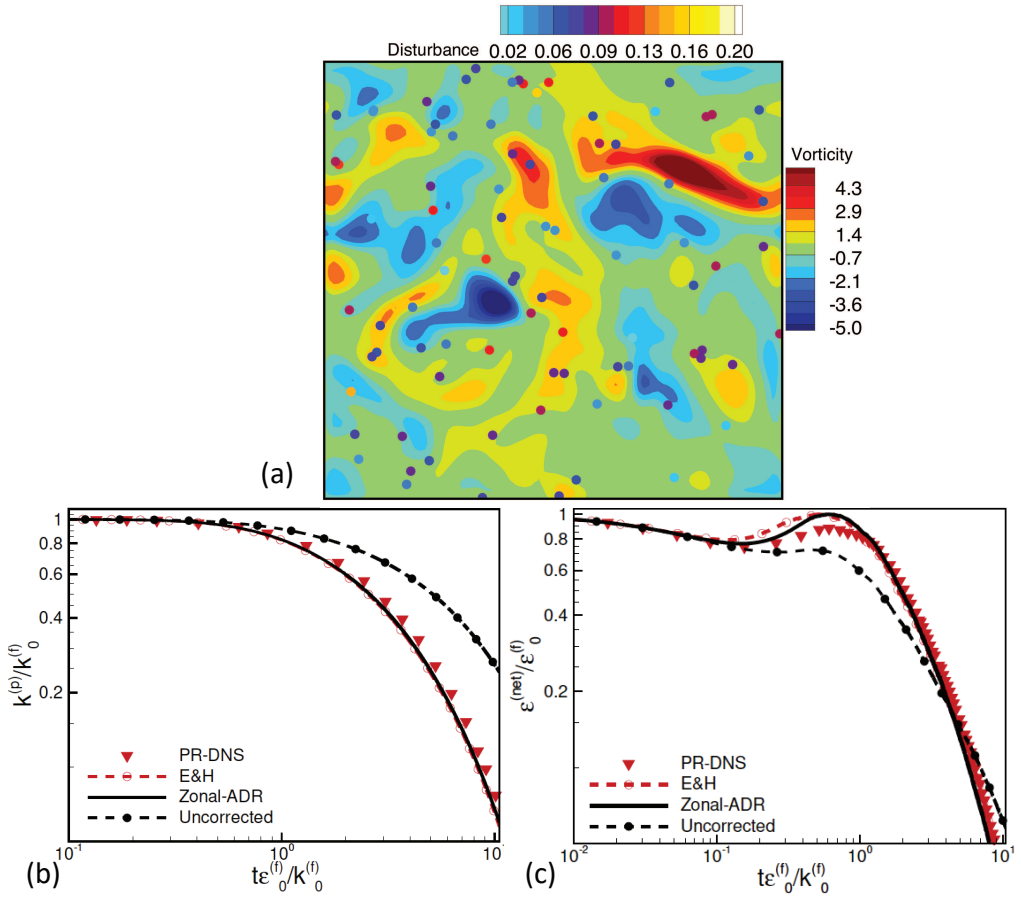

FIGURE 3. Decaying isotropic turbulence laden with Kolmogorov-scale particles: (a) snapshot of out-of-plane vorticity contours with scatter plot of particles colored by the disturbance velocity magnitude, (b) normalized particle kinetic energy, and (c) normalized net dissipation rate. Predictions with no model, Zonal-ADR, and Esmaily & Horwitz (2018) model (E&H) compared against the PR-DNS data by Mehrabadi *et al.* (2018) are shown.

underpredicted when using the grid-based Roma interpolation, whereas with correction, it closely follows the PR-DNS data.

5. Conclusions

A novel Zonal-ADR method is developed that solves a model equation for the self-disturbance created by a particle in point-particle simulations in a small region surrounding each particle. An overset grid–based approach is used for the zonal solution. The approach is verified for a range of single- and multiple-particle systems to show good predictive capability. The approach is valid for a wide range of Reynolds numbers, wall-bounded flows, multiple-particle systems, any Euler-Lagrange interpolation kernel, and different hydrodynamic feedback forces. The zonal solution methodology of the ADR equation can be easily implemented in any flow solver and is suitable for parallelization using GPUs. Extensions to heat transfer and evaporation are possible and will be the focus of future study.

Acknowledgments

SVA is thankful for partial support from NSF awards #1851389, #2053248, and acknowledges several useful discussions with Prof. Marcus Herrmann, Dr. Suhas S. Jain, and Dr. Makrand Khanwale and communications with Dr. J. Horwitz, Dr. M. Mehrabadi, and Prof. S. Subramaniam about their PR-DNS data.

REFERENCES

Apte, S., Gorokhovski, M. & Moin, P. 2003 LES of atomizing spray with stochastic modeling of secondary breakup. *Int. J. Multiph. Flow.* **29**, 1503–1522.

Balachandar, S., Liu, K. & Lakhote, M. 2019 Self-induced velocity correction for improved drag estimation in Euler–Lagrange point-particle simulations. *J. Comput. Phys.* **376**, 160–185.

Esmaily, M. & Horwitz, J. 2018 A correction scheme for two-way coupled point-particle simulations on anisotropic grids. *J. Comput. Phys.* **375**, 960–982.

Evrard, F., Denner, F. & van Wachem, B. 2020 Euler–Lagrange modelling of dilute particle-laden flows with arbitrary particle-size to mesh-spacing ratio. *J. Comput. Phys.* **8**, 100078.

Finn, J. R., Li, M. & Apte, S. V. 2016 Particle based modelling and simulation of natural sand dynamics in the wave bottom boundary layer. *J. Fluid Mech.* **796**, 340–385.

Ganguli, S. & Lele, S. K. 2019 Drag of a heated sphere at low Reynolds numbers in the absence of buoyancy. *J. Fluid Mech.* **869**, 264–291.

Gualtieri, P., Picano, F., Sardina, G. & Casciola, C. M. 2015 Exact regularized point particle method for multiphase flows in the two-way coupling regime. *J. Fluid Mech.* **773**, 520–561.

Horwitz, J., Iaccarino, G., Eaton, J. & Mani, A. 2022 The discrete Green's function paradigm for two-way coupled Euler–Lagrange simulation. *J. Fluid Mech.* **931**, A3.

Horwitz, J. & Mani, A. 2018 Correction scheme for point-particle models applied to a nonlinear drag law in simulations of particle-fluid interaction. *Int. J. Multiph. Flow.* **101**, 74–84.

Ireland, P. J. & Desjardins, O. 2017 Improving particle drag predictions in Euler–Lagrange simulations with two-way coupling. *J. Comput. Phys.* **338**, 405–430.

Liu, K., Lakhote, M. & Balachandar, S. 2019 Self-induced temperature correction for inter-phase heat transfer in Euler–Lagrange point-particle simulation. *J. Comput. Phys.* **396**, 596–615.

Maxey, M. R. 1987 The gravitational settling of aerosol particles in homogeneous turbulence and random flow fields. *J. Fluid Mech.* **174**, 441–465.

Mehrabadi, M., Horwitz, J., Subramaniam, S. & Mani, A. 2018 A direct comparison of particle-resolved and point-particle methods in decaying turbulence. *J. Fluid Mech.* **850**, 336–369.

Paksereshт, P. & Apte, S. V. 2021 A disturbance corrected point-particle approach for two-way coupled particle-laden flows on arbitrary shaped grids. *J. Comput. Phys.* **439**, 110381.

Paksereshт, P., Esmaily, M. & Apte, S. V. 2020 A correction scheme for wall-bounded two-way coupled point-particle simulations. *J. Comput. Phys.* **420**, 109711.

Pope, S. B. 2000 *Turbulent Flows*. Cambridge University Press, Cambridge, MA.

Roma, A. M., Peskin, C. S. & Berger, M. J. 1999 An adaptive version of the immersed boundary method. *J. Comput. Phys.* **153**, 509–534.